Stability in Lagrangian and Semi-Lagrangian Reproducing Kernel Discretizations Using Nodal Integration in Nonlinear Solid Mechanics

Jiun-Shyan Chen[1] and Youcai Wu[2]

[1]*Civil & Environmental Engineering, 5713 Boelter Hall, UCLA, Los Angeles, CA 90095, U.S.A.; E-mail: jschen@seas.ucla.edu*
[2]*Karagozian & Case, 2550 N Hollywood Way, Suite 500, Burbank, CA 91505, U.S.A.*

Abstract. Stability analyses of Lagrangian and Semi-Lagrangian Reproducing Kernel (RK) approximations for nonlinear solid mechanics are performed. It is shown that the semi-Lagrangian RK discretization yields a convective term resulting from the non-conservative coverage of material points under the kernel support. The von Neumann stability analysis shows that the discrete equations of both Lagrangian and semi-Lagrangian discretizations are stable when they are integrated using stabilized conforming nodal integration. On the other hand, integrating the semi-Lagrangian discretization with a direct nodal integration yields an unstable discrete system which resembles the tensile instability in SPH. Under the framework of semi-Lagrangian discretization, it is shown that the inclusion of convective term yields a more stable discrete system compared to the semi-Lagrangian discretization without convective term as was the case in SPH.

Key words: Semi-Lagrangian, reproducing kernel, nodal integration, meshfree method, large deformation.

1 Introduction

Particle and meshfree methods offer considerable advantages over the finite element method in modeling large deformation solid mechanics problems, where mesh entanglement difficulty in the finite element method can be considerably reduced. Smoothed Particle Hydrodynamics (SPH), originally introduced for astrophysics [12, 15] has been extended to model large deformation problems in solids [16, 19]. SPH method, however, exhibits tensile instability [3, 17, 20]. This tension instability has been corrected by the employment of Lagrangian kernel under the framework of reproducing kernel particle method (RKPM) [5, 6]. The Lagrangian kernel based RKPM has been applied to path-independent hyperelasticity [4, 6, 11] and

M.A. Leitão et al. (eds), Advances in Meshfree Techniques, 55–76.

path-dependent plasticity [5–8] large deformation problems. The Lagrangian kernel based meshfree methods in nonlinear solid mechanics, however, have their inherent difficulty due to the regularity requirement of the deformation gradient needed for inverse mapping from deformed configuration to undeformed configuration. A semi-Lagrangian formulation under the framework of reproducing kernel particle method is proposed herein for extremely large deformation solid mechanics problems. Semi-Lagrangian discretization defines kernel function distance measure in the deformed configuration and thus avoids the need for inverse mapping from deformed to undeformed configurations.

The main difference between Lagrangian kernel and semi-Lagrangian kernel is due to the definition of distance measure between point of evaluation and discrete points. The Lagrangian kernel defined at the material discrete points yields vanishing material time derivative of the Lagrangian kernel. On the other hand, material time derivative of the semi-Lagrangian kernel does not vanish due to the advection of materials covered under the kernel support during material deformation. Consequently, nodal mass is not conservative when a continuum is discretized by the semi-Lagrangian kernel, and an additional convective term appears in the conservation laws. Note that SPH is semi-Lagrangian in nature, but it was formulated without considering the above mentioned non-conservative nodal mass and the convective effect in the conservation laws.

Two types of instabilities have been discussed in meshfree literatures: the tensile instability and the rank instability. The tensile instability in SPH has been analyzed by Swegle et al. [20]. Stability analysis of element free Galerkin (EFG) method using Lagrangian and Eulerian kernels has been conducted [1, 2] and the method has been applied to problems with moderate deformations [18]. Belytschko and Xiao [1] showed that tensile instability can be resolved by using a Lagrangian kernel [6]. Other remedies for tensile instability in SPH such as the conservative smoothing approach by Guenther et al. [22] and Swegle et al. [23], the stress point approach by Dyka and Ingel [21], and an artificial stress approach by Monaghan [17] have been proposed. The rank instability due to direct nodal integration (DNI) has been pointed out by Chen et al. [9, 10] and a stabilized conforming nodal integration (SCNI) has been proposed.

In this work, stability analysis of Lagrangian and semi-Lagrangian Galerkin meshfree formulations will be performed. The effects of domain integration using direct nodal integration and stabilized conforming nodal integration on numerical stability will also be analyzed. The remaining of the paper is arranged as follows. An overview of Lagrangian discretization using reproducing kernel (RK) approximation is given in Section 2. In Section 3, the semi-Lagrangian kernel and the corresponding RK shape functions are presented, and the semi-Lagrangian discretizations of equation of motion are derived. The convective effect resulting from the non-conservative nature of semi-Lagrangian kernel is also identified. Von Neumann stability analyses

of Lagrangian and semi-Lagrangian discrete equations integrated by SCNI and DNI are carried out in Section 4. Conclusion remarks are given in Section 5.

2 Lagrangian Reproducing Kernel Discretization

2.1 Reproducing Kernel (RK) Approximation

Let the problem domain Ω be discretized into a set of NP points $\{\mathbf{x}_1, \mathbf{x}_2, \ldots, \mathbf{x}_{NP}\}$, where $\mathbf{x}_I$ is the location of node I and NP denotes the total number of points. The variable, for example, displacement $u_i(\mathbf{x})$ in solid mechanics, is approximated by:

$$u_i^h(\mathbf{x}) = \sum_{I=1}^{NP} \Psi_I(\mathbf{x}) d_{iI}, \tag{1}$$

where $u_i^h(\mathbf{x})$ is the approximation of $u_i(\mathbf{x})$, and Ψ_I and d_{iI} are the shape functions and their associated coefficients, respectively. Under the framework of reproducing kernel approximation, the shape function $\Psi_I(\mathbf{x})$ is expressed as:

$$\Psi_I(\mathbf{x}) = \Big(\sum_{i+j=0}^{n} (x_1 - x_{1I})^i (x_2 - x_{2I})^i \; b_{ij}(\mathbf{x}) \Big) \phi_a(\mathbf{x} - \mathbf{x}_I), \tag{2}$$

where $\phi_a(\mathbf{x} - \mathbf{x}_I)$ is a kernel function that defines the smoothness and locality of the approximation with a compact support a, which is the radius of the support. The unknown coefficients $\mathbf{b}(\mathbf{x})$ in Equation (2) are obtained by enforcing the following nth order reproducing conditions:

$$\sum_{I=1}^{NP} \Psi_I(\mathbf{x}) \; x_{1I}^{\alpha} \; x_{2I}^{\beta} = x_1^{\alpha} x_2^{\beta}, \quad \alpha + \beta = 0, 1, 2, \ldots, n. \tag{3}$$

Upon solving $b_{ij}(\mathbf{x})$ from Equation (3), the shape functions are obtained:

$$\Psi_I(\mathbf{x}) = \mathbf{H}^T(\mathbf{0}) \mathbf{M}^{-1}(\mathbf{x}) \mathbf{H}(\mathbf{x} - \mathbf{x}_I) \phi_a(\mathbf{x} - \mathbf{x}_I), \tag{4}$$

where

$$\mathbf{H}^T(\mathbf{x} - \mathbf{x}_I) = [1 \quad x_1 - x_{1I} \quad x_2 - x_{2I} \quad (x_1 - x_{1I})^2 \quad \ldots \quad \ldots \quad (x_2 - x_{2I})^n], \tag{5}$$

$$\mathbf{M}(\mathbf{x}) = \sum_{I=1}^{NP} \mathbf{H}(\mathbf{x} - \mathbf{x}_I) \mathbf{H}^T(\mathbf{x} - \mathbf{x}_I) \phi_a(\mathbf{x} - \mathbf{x}_I). \tag{6}$$

2.2 Lagrangian Description and Discretization of Equation of Motion

In solid mechanics large deformation problems, material motion from undeformed (initial) domain Ω_X to deformed (current) domain Ω_x has to be defined. Consider a material particle originally located at $\mathbf{X}$ in the undeformed domain Ω_X . Under certain action this material particle is moved to $\mathbf{x}$ at time t in the deformed domain Ω_x. The motion of the material particle $\mathbf{X}$ is described by a mapping function $\mathbf{x} = \varphi(\mathbf{X}, t)$, and $\mathbf{u}(\mathbf{X}, t) = \mathbf{x}(\mathbf{X}, t) - \mathbf{X}$ is the displacement vector associated with material particle originally positioned at $\mathbf{X}$. In Lagrangian description, the weak form of equation of motion expressed in the undeformed domain Ω_X is expressed as:

$$\int_{\Omega_X} \delta u_i \rho^0 \, \ddot{u}_i \, \mathrm{d}\Omega + \int_{\Omega_X} \delta F_{ij} P_{ji} \, \mathrm{d}\Omega = \int_{\Omega_X} \delta u_i b_i^0 \, \mathrm{d}\Omega + \int_{\Gamma_X^h} \delta u_i h_i^0 \, \mathrm{d}\Gamma, \quad (7)$$

where $F_{ij} = \partial x_i / \partial X_j$ is the deformation gradient, P_{ij} is the first Piola–Kirchhoff stress which in general is a function of F_{ij} and its rate, J is the determinant of the deformation gradient, ρ^0 is the initial density, b_i^0 is the body force defined in the undeformed domain Ω_X, and h_i^0 is the surface traction mapped onto the undeformed traction (natural) boundary Γ_X^h.

In the Lagrangian discretization, the reproducing kernel approximation of material displacements is expressed as [5, 6]:

$$u_i^h(\mathbf{X}, t) = \sum_{I=1}^{NP} \Psi_I^X(\mathbf{X}) d_{iI}(t), \quad (8)$$

where $\mathbf{X}$ is the material coordinate defined in the undeformed domain (configuration). Based on RK approximation, the Lagrangian shape function is expressed as

$$\Psi_I^X(\mathbf{X}) = \mathbf{H}^T(\mathbf{0}) \mathbf{M}^{-1}(\mathbf{X}) \mathbf{H}(\mathbf{X} - \mathbf{X}_I) \phi_a(\mathbf{X} - \mathbf{X}_I), \quad (9)$$

where the basis functions are defined as

$$\mathbf{H}^T(\mathbf{X} - \mathbf{X}_I) = [1 \quad X_1 - X_{1I} \quad X_2 - X_{2I} \quad \ldots \quad (X_2 - X_{2I})^N] \quad (10)$$

and the moment matrix is computed by

$$\mathbf{M}(\mathbf{X}) = \sum_{I=1}^{NP} \mathbf{H}(\mathbf{X} - \mathbf{X}_I) \mathbf{H}^T(\mathbf{X} - \mathbf{X}_I) \phi_a(\mathbf{X} - \mathbf{X}_I). \quad (11)$$

An example of kernel function is

$$\phi_a(z) = \begin{cases} \frac{2}{3} - 4z^2 + 4z^3 & 0 \le z \le \frac{1}{2} \\ \frac{4}{3} - 4z + 4z^2 - \frac{4}{3}z^3 & \frac{1}{2} < z \le 1 \\ 0 & z > 1. \end{cases} \quad z = \frac{\|\mathbf{X} - \mathbf{X}_I\|}{a} \quad (12)$$

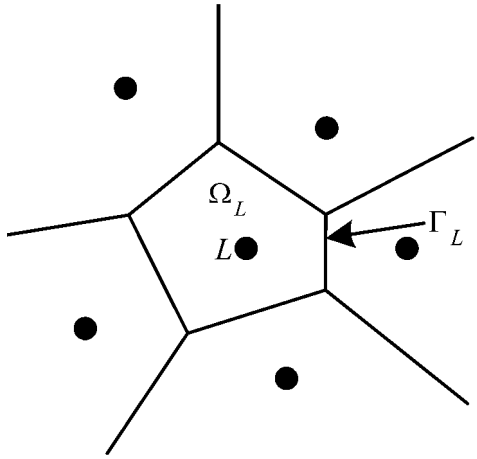

Fig. 1. Representative integration domain for SCNI.

The shape functions $\Psi_I^X(\mathbf{X})$ formulated using material coordinate $\mathbf{X}$ in the undeformed domain Ω_X are called the Lagrangian shape functions.

A stabilized conforming nodal integration (SCNI) [9] has been introduced for the integration of weak form to achieve computational efficiency and stability. Linear exactness in the Galerkin approximation requires (1) first order completeness of the trial and test functions, and (2) a domain integration that satisfies integration constraints. To meet integration constraints for nodal integration of Equation (7) using the deformation gradient as the primary kinematic variable, a smoothing of deformation gradient at a nodal point with material coordinate $\mathbf{X}_L$ has been considered [10]:

$$\bar{F}_{ij}(\mathbf{X}_L) = \frac{1}{A_L}\int_{\Omega_L} F_{ij}\,\mathrm{d}\Omega = \frac{1}{A_L}\int_{\Omega_L}\frac{\partial u_i}{\partial X_j}\,\mathrm{d}\Omega + \delta_{ij}, \quad A_L = \int_{\Omega_L}\mathrm{d}\Omega, \tag{13}$$

where Ω_L is the nodal representative domain of $\mathbf{X}_L$ in the undeformed configuration as shown in Figure 1. Applying the divergence theorem at the undeformed configuration yields

$$\bar{F}_{ij}(\mathbf{X}_L) = \frac{1}{A_L}\int_{\Gamma_L} u_i N_j\,\mathrm{d}\Gamma + \delta_{ij} = \bar{e}_{ij}(\mathbf{X}_L) + \delta_{ij}, \tag{14}$$

where

$$\bar{e}_{ij}(\mathbf{X}_L) = \frac{1}{A_L}\int_{\Gamma_L} u_i N_j\,\mathrm{d}\Gamma. \tag{15}$$

In Equation (15), Γ_L is the boundary of Ω_L as shown in Figure 1, and N_i is the surface normal of Γ_L. Generally, a Voronoi diagram is employed to generate the representative domain. Introducing a Lagrangian shape function into Equation (15) yields

$$\bar{e}_{ij}(\mathbf{X}_L) = \sum_I \bar{b}^L_{jI}\, d_{iI}, \tag{16}$$

where

$$\bar{b}^L_{iI} = \frac{1}{A_L}\int_{\Gamma_L} \Psi^X_I N_i \, \mathrm{d}\Gamma. \tag{17}$$

It has been shown that by introducing linear basis functions in material coordinate in the reproducing kernel approximation (Equations (9)–(11)), and by employing the above smoothed deformation gradient (Equations (14)–(17)) in the static Lagrangian equilibrium equation integrated by nodal integration, exact solution can be obtained in large deformation problems with homogeneous constant deformation field [10], which is the large deformation version of linear patch test. The corresponding discrete equation of Equation (7) is:

$$\mathbf{M}\ddot{\mathbf{u}} = \mathbf{f}^{\text{ext}} - \mathbf{f}^{\text{int}}, \tag{18}$$

where

$$\mathbf{M}_{IJ} = \sum_L \rho_0 \Psi^X_I(\mathbf{X}_L)\Psi^X_J(\mathbf{X}_L)\mathbf{I}A_L, \tag{19}$$

$$\mathbf{f}^{\text{ext}}_I = \sum_K \Psi^X_I(\hat{\mathbf{X}}_K)\mathbf{h}^0(\hat{\mathbf{X}}_K)W_K + \sum_L \Psi^X_I(\mathbf{X}_L)\mathbf{b}^0(\mathbf{X}_L)A_L, \tag{20}$$

$$\mathbf{f}^{\text{int}}_I = \sum_L \bar{\mathbf{B}}^T_I(\mathbf{X}_L)\mathbf{P}(\mathbf{X}_L)A_L, \tag{21}$$

$$\bar{\mathbf{B}}_I(\mathbf{X}_L) = \begin{bmatrix} \bar{b}^L_{1I} & 0 \\ 0 & \bar{b}^L_{2I} \\ \bar{b}^L_{2I} & 0 \\ 0 & \bar{b}^L_{1I} \end{bmatrix}, \quad \mathbf{P}(\mathbf{X}_L) = \begin{bmatrix} P_{11}(\mathbf{X}_L) \\ P_{22}(\mathbf{X}_L) \\ P_{12}(\mathbf{X}_L) \\ P_{21}(\mathbf{X}_L) \end{bmatrix}, \tag{22}$$

$$\bar{b}^L_{iI} = \frac{1}{A_L}\int_{\Gamma_L} \Psi^X_I N_i \, \mathrm{d}\Gamma, \quad A_L = \int_{\Omega_L} \mathrm{d}\Omega, \tag{23}$$

where $\mathbf{X}_L$ and A_L are the nodal point position and the corresponding weight associated with domain integration in the undeformed domain Ω_X, $\hat{\mathbf{X}}_K$, and W_K are the nodal point position and weight associated with boundary integration on the undeformed natural boundary Γ^h_X, and Γ_L and N_i are the boundary and surface normal of the nodal representative domain Ω_L in the undeformed configuration. Note that the area of nodal representative domain A_L is used as the weight of nodal integration.

3 Semi-Lagrangian Reproducing Kernel Discretization

3.1 Semi-Lagrangian RK Shape Function

For problems involving path-dependent materials such as materials deformed in plastic deformation, the internal energy is expressed as

$$\int_{\Omega_X} \frac{\partial \delta u_i}{\partial X_k} P_{ki} \, \mathrm{d}\Omega = \int_{\Omega_X} \frac{\partial \delta u_i}{\partial X_k} \, F_{kj}^{-1} \sigma_{ij} \, J \, \mathrm{d}\Omega, \tag{24}$$

where σ_{ij} is Cauchy stress. Cauchy stress calculation requires the spatial derivative of displacements approximated by Lagrangian shape functions, and thus the following chain rule is employed:

$$\frac{\partial \Psi_I^X(\mathbf{X})}{\partial x_i} = \frac{\partial \Psi_I^X(\mathbf{X})}{\partial X_j} \frac{\partial X}{\partial x_i} = \frac{\partial \Psi_I^X(\mathbf{X})}{\partial X_j} F_{ji}^{-1}, \tag{25}$$

where $\mathbf{F}^{-1}$ is obtained by taking a direct inverse of $\mathbf{F}$.

It is clear that this Lagrangian formulation in Equations (24) and (25) breaks down when the mapping $\mathbf{x} = \varphi(\mathbf{X}, t)$ or the inverse mapping $\mathbf{X} = \varphi^{-1}(\mathbf{x}, t)$ is no longer regular (one-to-one). This happens in problems involve situations such as new free surface formation in damage evolution or free surface closure that commonly exists in materials processing, earth moving, and penetration processes. To circumvent this difficulty, a semi-Lagrangian discretization is proposed.

As has been mentioned, the distance measure, $z = \|\mathbf{X} - \mathbf{X}_I\|/a$ for Lagrangian kernel $\phi_a(z)$ is defined in the undeformed configuration. Therefore, the kernel support covers the same set of material particles before and after deformation in the Lagrangian discretization. Similar to the Lagrangian discretization, in semi-Lagrangian discretization the discrete meshfree points follow the material motion, however, the distance measure $z = \|\mathbf{x} - \mathbf{x}(\mathbf{X}_I, t)\|/a$ in the semi-Lagrangian kernel $\phi_a(z)$ is defined in the deformed configuration. Under this definition, the material particles covered under the kernel support vary during material deformation. These two different kernel functions are compared as follows:

$$\phi_a(z) : \begin{cases} \text{Lagrangian kernel:} \quad z = \|\mathbf{X} - \mathbf{X}_I\|/a, \\ \text{Semi-Lagrangian kernel:} \quad z = \|\mathbf{x} - \mathbf{x}(\mathbf{X}_I, t)\|/a. \end{cases} \tag{26}$$

Figure 2 schematically compares kernel supports in Lagrangian and semi-Lagrangian kernels.

As shown in Figure 2, Lagrangian kernel deforms with the material, and the kernel support covers the same group of material particles at all time. For the semi-Lagrangian kernel, in general, material particles can move in and out of the kernel support during the deformation processes.

In semi-Lagrangian discretization, the discrete points follow the material motion, i.e., $\mathbf{x}_I = \mathbf{x}(\mathbf{X}_I, t)$, whereas the approximation is formulated in the current configuration in the following form

$$u_i(\mathbf{x}, t) = \sum_{I=1}^{NP} \Psi_I(\mathbf{x}) d_{iI}(t), \tag{27}$$

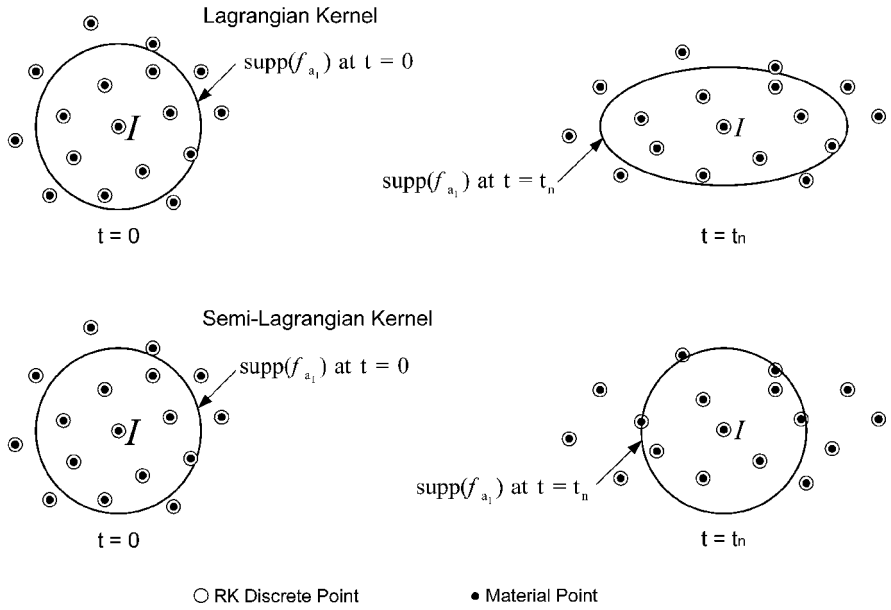

Fig. 2. Comparison of Lagrangian and semi-Lagrangian kernels.

where the semi-Lagrangian shape function $\psi_I(\mathbf{x})$ is constructed based on (i) the current position of material points and (ii) basis functions defined in the current configuration as follows

$$\Psi_I(\mathbf{x}) = \sum_{i+j=0}^{n} [(x_1 - x_1(\mathbf{X}_I, t))^i (x_2 - x_2(\mathbf{X}_I, t))^j \; b_{ij}(\mathbf{x})]\phi_a(\mathbf{x} - \mathbf{x}(\mathbf{X}_I, t)). \quad (28)$$

The coefficients $b_{ij}(\mathbf{x})$ are constructed by imposing the following semi-Lagrangian reproducing conditions

$$\sum_{I=1}^{NP} \Psi_I(\mathbf{x}) x_1(\mathbf{X}_I, t)^i \; x_2(\mathbf{X}_I, t)^j = x_1^i x_2^j, \quad i + j = 0, 1, 2, \ldots, n \; . \quad (29)$$

Solving $b_{ij}(\mathbf{x})$ from Equation (29) yields the following semi-Lagrangian shape function:

$$\Psi_I(\mathbf{x}) = C(\mathbf{x}; \mathbf{x} - \mathbf{x}(\mathbf{X}_I, t))\phi_a(\mathbf{x} - \mathbf{x}(\mathbf{X}_I, t)), \quad (30)$$

where

$$C(\mathbf{x}; \mathbf{x} - \mathbf{x}(\mathbf{X}_I, t)) = \mathbf{H}^T(\mathbf{0})\mathbf{M}^{-1}(\mathbf{x})\mathbf{H}(\mathbf{x} - \mathbf{x}(\mathbf{X}_I, t)), \quad (31)$$

$$\mathbf{M}(\mathbf{x}) = \sum_{I=1}^{NP} \mathbf{H}(\mathbf{x} - \mathbf{x}(\mathbf{X}_I, t))\mathbf{H}^T(\mathbf{x} - \mathbf{x}(\mathbf{X}_I, t))\phi_a(\mathbf{x} - \mathbf{x}(\mathbf{X}_I, t)), \tag{32}$$

$$\mathbf{H}^T(\mathbf{x} - \mathbf{x}(\mathbf{X}_I, t)) = [1 \quad x_1 - x_1(\mathbf{X}_I, t) \quad x_2 - x_2(\mathbf{X}_I, t) \quad \dots \quad (x_2 - x_2(\mathbf{X}_I, t))^n]. \tag{33}$$

3.2 Material Time Derivatives

The difference between Lagrangian and semi-Lagrangian approximations can be observed in the material time derivative of Lagrangian and semi-Lagrangian kernels:

1. Lagrangian kernel: $$\dot{\phi}_a\left(\frac{\|\mathbf{X} - \mathbf{X}_I\|}{a}\right) = 0 \tag{34}$$

2. Semi-Lagrangian kernel: $$\dot{\phi}_a\left(\frac{\|\mathbf{x} - \mathbf{x}(\mathbf{X}_I, t)\|}{a}\right) \tag{35}$$

$$= \phi'_a\left(\frac{\|\mathbf{x} - \mathbf{x}(\mathbf{X}_I, t)\|}{a}\right) \frac{\mathbf{n} \cdot (\mathbf{v} - \mathbf{v}_I)}{a},$$

where

$$\dot{(\,)} = \left.\frac{\partial(\,)}{\partial t}\right|_{[\mathbf{X}]} \quad \text{is the material time derivative, and}$$

$$\mathbf{n} = \frac{\mathbf{x} - \mathbf{x}(\mathbf{X}_I, t)}{\|\mathbf{x} - \mathbf{x}(\mathbf{X}_I, t)\|}. \tag{36}$$

The term $\mathbf{n} \cdot (\mathbf{v} - \mathbf{v}_I)$ in Equation (35) is the projection of relative velocity between point of evaluation ($\mathbf{x}$) and grid point ($\mathbf{x}(\mathbf{X}_I, t)$) onto the kernel support radial direction centered at $\mathbf{x}(\mathbf{X}_I, t)$, and it represents the relative motion between the neighboring material $\mathbf{x}$ and the kernel support center point $\mathbf{x}(\mathbf{X}_I, t)$ as shown in Figure 3. Positive value of $\mathbf{n} \cdot (\mathbf{v} - \mathbf{v}_I)$ indicates $\mathbf{x}$ moving away from $\mathbf{x}(\mathbf{X}_I, t)$, and negative value of $\mathbf{n} \cdot (\mathbf{v} - \mathbf{v}_I)$ indicates $\mathbf{x}$ moving towards $\mathbf{x}(\mathbf{X}_I, t)$.

3.3 Semi-Lagrangian Discrete Equation of Motion

The semi-Lagrangian discrete equation of motion is obtained by employing the following weak form of equation of motion expressed in the deformed domain Ω_x:

$$\int_{\Omega_x} \delta u_{(i,j)} \sigma_{ij} \, \mathrm{d}\Omega + \int_{\Omega_x} \delta u_i \rho \ddot{u}_i \, \mathrm{d}\Omega = \int_{\Omega_x} \delta u_i b_i \, \mathrm{d}\Omega + \int_{\Gamma_x^h} \delta u_i h_i \, \mathrm{d}\Gamma, \tag{37}$$

where σ_{ij} is the Cauchy stress, $u_{(i,j)} = (\partial u_i/\partial x_j + \partial u_j/\partial x_i)/2$, ρ is the density at the current state, b_i is the body force defined in the deformed domain Ω_x, and h_i is

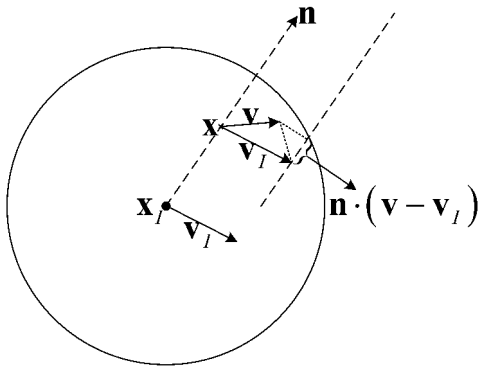

Fig. 3. Relative motion between neighboring material $\mathbf{x}$ and kernel support center point $\mathbf{x}_I = \mathbf{x}(\mathbf{X}_I, t)$.

the surface traction defined on the deformed traction boundary Γ_x^h. Let the velocity v_i be approximated by semi-Lagrangian shape functions,

$$v_i^h(\mathbf{x}, t) = \sum_{I=1}^{NP} \Psi_I(\mathbf{x}) v_{iI}(t). \tag{38}$$

The corresponding semi-Lagrangian approximation of acceleration is given as

$$\ddot{u}_i^h(\mathbf{x}, t) = \dot{v}_i^h(\mathbf{x}, t) = \sum_{I=1}^{NP} (\Psi_I(\mathbf{x}) \dot{v}_{iI}(t) + \Psi_I^*(\mathbf{x}) v_{iI}(t)), \tag{39}$$

where $\Psi_I^*(\mathbf{x})$ is the correction due to time rate of the semi-Lagrangian kernel $\dot{\phi}_a$

$$\Psi_I^*(\mathbf{x}) = C(\mathbf{x}; \mathbf{x} - \mathbf{x}(\mathbf{X}_I, t)) \dot{\phi}_a(\mathbf{x} - \mathbf{x}(\mathbf{X}_I, t)). \tag{40}$$

Substituting Equations (38) and (39) into formula (37), and considering strain smoothing of $u_{(i,j)}$ with similar procedures discussed in Section 2, the following discrete equation is obtained

$$\mathbf{M}\dot{\mathbf{v}} + \mathbf{N}\mathbf{v} = \mathbf{f}^{\text{ext}} - \mathbf{f}^{\text{int}}, \tag{41}$$

where

$$\mathbf{M}_{\mathbf{IJ}} = \sum_L \rho(\mathbf{x}(\mathbf{X}_L, t)) \Psi_I(\mathbf{x}(\mathbf{X}_L, t)) \Psi_J(\mathbf{x}(\mathbf{X}_L, t)) \mathbf{I} a_L, \tag{42}$$

$$\mathbf{N}_{IJ} = \sum_L \rho(\mathbf{x}(\mathbf{X}_L, t)) \Psi_I(\mathbf{x}(\mathbf{X}_L, t)) \Psi_J^*(\mathbf{x}(\mathbf{X}_L, t)) \mathbf{I} a_L, \tag{43}$$

$$\mathbf{f}_I^{\text{ext}} = \sum_K \Psi_I(\mathbf{x}(\hat{\mathbf{X}}_K, t))\mathbf{h}(\mathbf{x}(\hat{\mathbf{X}}_K, t))w_k + \sum_L \Psi_I(\mathbf{x}(\mathbf{X}_L, t))\mathbf{b}(\mathbf{x}(\mathbf{X}_L, t))a_L \quad (44)$$

$$\mathbf{f}_I^{\text{int}} = \sum_L \bar{\mathbf{B}}_I^T(\mathbf{x}(\mathbf{X}_L, t))\,\boldsymbol{\Xi}(\mathbf{x}(\mathbf{X}_L, t))a_L, \quad (45)$$

$$\bar{\mathbf{B}}_I(\mathbf{x}(\mathbf{X}_L, t) = \begin{bmatrix} \bar{b}_{1I}^L & 0 \\ 0 & \bar{b}_{2I}^L \\ \bar{b}_{2I}^L & \bar{b}_{1I}^L \end{bmatrix} \qquad \boldsymbol{\Xi}(\mathbf{x}(\mathbf{X}_L, t) = \begin{bmatrix} \sigma_{11}(\mathbf{x}(\mathbf{X}_L, t)) \\ \sigma_{22}(\mathbf{x}(\mathbf{X}_L, t)) \\ \sigma_{12}(\mathbf{x}(\mathbf{X}_L, t)) \end{bmatrix}, \quad (46)$$

$$\bar{b}_{iI}^L = \frac{1}{a_L}\int_{\gamma_L} \Psi_I n_i \, \mathrm{d}\Gamma \qquad a_L = \int_{\omega_L} \mathrm{d}\Omega, \quad (47)$$

where $\mathbf{x}(\mathbf{X}_L, t)$ and a_L are the nodal point position and the corresponding weight associated with domain integration in the deformed domain Ω_x, respectively, $\mathbf{x}(\hat{\mathbf{X}}_K, t)$ and w_k are the nodal point position and weight associated with boundary integration on the deformed natural boundary Γ_x^h, respectively, and γ_L and n_i are the boundary and surface normal of the nodal representative domain ω_L in the deformed configuration, respectively. The second term on the left hand side of Equation (41) is a convective term resulting from the material time derivative of the semi-Lagrangian kernel function.

4 Stability Analysis of Lagrangian and Semi-Lagrangian Discrete Equations

Von Neumann stability analyses of Lagrangian and semi-Lagrangian discrete equations are presented in this section. The following notations are used in stability analysis:

$$\begin{aligned} &C(h) = C(x_I; x_{I+1} - x_I) && \phi_a(h) = \phi_a(x_{I+1} - x_I) \\ &C(h/2) = C(x_I; x_{I+1/2} - x_I) && \phi_a(h/2) = \phi_a(x_{I+1/2} - x_I) \\ &\Psi_I(0) = \Psi_I(x_I) && \Psi_I(h) = \Psi_I(x_{I+1}) \\ &\Psi_{I,x}(h) = \Psi_{I,x}(x_{I+1}) && \Psi_{I,xx}(h) = \Psi_{I,xx}(x_{I+1}). \end{aligned}$$

where $h = \Delta x$ is the constant nodal spacing.

4.1 Lagrangian Discrete Equation of Motion Integrated by SCNI

The Lagrangian discrete equation of motion in one-dimension can be expressed as:

$$\mathbf{M}\ddot{\mathbf{u}} = \mathbf{f}^{\text{ext}} - \mathbf{f}^{\text{int}}, \quad (48)$$

where

$$F_I^{\text{int}} = \int_{\Omega_x} \Psi_I^X(X)_{,X}\ P\ \mathrm{d}\Omega, \tag{49}$$

$$F_I^{\text{ext}} = \int_{\Omega_x} \Psi_I^X(X) b^0\ \mathrm{d}\Omega + \Psi_I^X(X) h^0 \Big|_{\Gamma_X^h}. \tag{50}$$

By employing SCNI, Equation (49) can be written as

$$f_I^{\text{int}} = \sum_{L=I}^{NP} \bar{b}_I^L P(X_L) A_L, \tag{51}$$

where $\bar{b}_I^L$ is the smoothed gradient:

$$\bar{b}_I^L = \frac{1}{A_L}\left[\Psi_I^X(X_L^+) - \Psi_I^X(X_L^-)\right]. \tag{52}$$

In one-dimension, A_L is the length of nodal representative domain $\Omega_L =]X_L^-, X_L^+[$ for node L, and X_L^+ and X_L^- are the two end points of Ω_L. The first Piola–Kirchhoff stress P is defined as:

$$P = SF. \tag{53}$$

Here S is the second Piola–Kirchhoff stress obtained by

$$\Delta S = C^{\text{SE}} \Delta E \tag{54}$$

and the Green strain E is given as

$$E = \frac{1}{2}(F^2 - 1). \tag{55}$$

Further considering lumped mass, the Lagrangian discrete equation of motion at a node I can be written as

$$m_I \ddot{u}_I = f_I^{\text{ext}} - f_I^{\text{int}} \qquad \text{no summation on } I. \tag{56}$$

Assuming small perturbation in displacement, the perturbation equation of Equation (56) reads [2]:

$$m_I \ddot{\tilde{u}}_I = -\tilde{f}_I^{\text{int}}. \tag{57}$$

From Equation (51), we have

$$\tilde{f}_I^{\text{int}} = \sum_{L=1}^{NP} \bar{b}_I^L\ \tilde{P}(X_L) A_L. \tag{58}$$

The perturbation of the first Piola–Kirchhoff stress is

$$\tilde{P}(X_L) = (C^{\mathrm{SE}} F^2 + S)\tilde{f}_L, \tag{59}$$

where

$$\tilde{f}_L = \left.\frac{\partial \tilde{u}}{\partial X}\right|_L = \sum_{I=1}^{NP} \bar{b}_I^L \, \tilde{u}_I. \tag{60}$$

Consider uniform particle distribution in an infinite domain, Equation (57) can be written as

$$\ddot{\tilde{u}}_I = -\frac{C^{\mathrm{SE}} F^2 + S}{\rho_0} \sum_{K=-m}^{m} \left[\bar{b}_I^{I+K} \sum_{J=-m}^{m} \bar{b}_I^{I-J} \, \tilde{u}_{I+J+K} \right], \tag{61}$$

where $m = \mathrm{int}(R + 0.5)$ is an integer determined by the normalized support size R (support size divided by nodal distance).

For plane wave, the perturbed displacement takes the form as

$$\tilde{u}_I = g e^{ikI\Delta x = i\omega t}, \tag{62}$$

where g is the amplitude of the perturbation, k is the wave number, ω is the frequency, and $\Delta x = h$ is the nodal spacing. Accordingly, the stability criterion is ω should be real. Substituting Equation (62) into Equation (61) yields:

$$\omega^2 = \frac{C^{\mathrm{SE}} F^2 + S}{\rho_0} \sum_{K=1}^{2m+1} \left[\hat{b}_K \sum_{L=1}^{2m+1} \hat{b}_L \cos(K - L)kh \right], \tag{63}$$

where

$$\hat{b}_K = \bar{b}_I^{I+K-m-1}. \tag{64}$$

Note that since uniform nodal spacing and infinite domain is considered, the index I is ignored in Equation (63) for notational simplicity. The frequency relations based on Equation (63) are shown in Figure 4 for various normalized support sizes, and $c^2 = (C^{\mathrm{SE}} F^2 + S)/\rho_0$. It is observed that the frequency is very close to zero near the cut-off point ($kh = \pi$) for the case with very large support size ($R = 3.5$). This implies that the stiffness matrix becomes more linearly dependent and ill conditioned when very large support size is used and this should be avoided.

4.2 Stability of Semi-Lagrangian Discrete Equation

In one-dimension, with the employment of lumped mass and nodal integration, the discrete equation of motion by the semi-Lagrangian approximation can be written as:

$$m_I \dot{v}_I + \sum_{J=I}^{NP} N_{IJ} v_J = f_I^{\mathrm{ext}} - f_I^{\mathrm{int}} \qquad \text{no summation on } I, \tag{65}$$

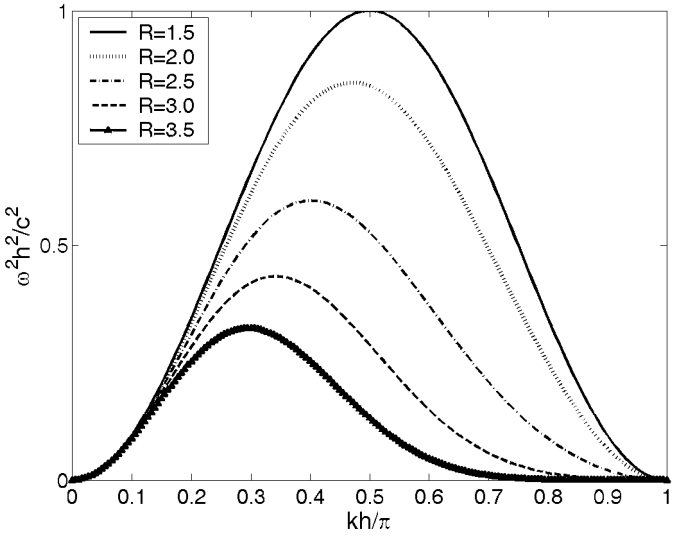

Fig. 4. Frequency characteristic of Lagrangian RK discretization with SCNI.

where

$$N_{IJ} = \sum_{K=1}^{NP} \rho(x_K)\Psi_I(x_K)\Psi_J^*(x_K)a_K, \tag{66}$$

$$f_I^{\text{int}} = \sum_{K=1}^{NP} \bar{B}_I(x_K)\sigma(x_K)a_K, \tag{67}$$

$$\Psi_I^*(x_K) = C(x_K; x_K - x_I)\dot{\phi}_a(x_K - x_I), \tag{68}$$

$$\sigma(x_K) = C^\sigma \varepsilon(x_K) = C^\sigma \sum_{J=1}^{NP} \bar{B}_J(x_K)u_J, \tag{69}$$

$$\dot{\phi}_a(x_K - x_I) = \phi_a'(x_K - x_I)\frac{n_{IK}(v_K - v_I)}{a}, \tag{70}$$

$$n_{IK} = \frac{x_K - x_I}{|x_K - x_I|}. \tag{71}$$

Here a_K is the length of nodal representative domain of node K, $x_K = x(X_K, t)$ is the current position of material point X_K, and C^σ is the material modulus. Note that $\bar{B}_I(x_K)$ is the gradient of shape function which takes the smoothed form (Equation (46)) if SCNI is used, and $\bar{B}_I(x_K) = \Psi_{I,x}(x_K)$ if a direct nodal integration (DNI) is employed.

4.2.1 Semi-Lagrangian Weak Form Integrated by Stabilized Conforming Nodal Integration (SCNI)

When SCNI is employed for domain integration, the smoothed shape function gradient following Equation (46) is

$$\bar{B}_I(x_K) = \bar{B}_I^K = \frac{1}{a_K}\left[\Psi_I(x_K^+) - \Psi_I(x_K^-)\right]. \tag{72}$$

In one-dimension, a_K is the length of nodal representative domain $\Omega_K =]x_K^-, x_K^+[$ for node K, and x_K^+ and x_K^- are the two end points of Ω_K. Under the assumption of small perturbation in displacement and velocity, the perturbation in nodal mass can be neglected, therefore, the perturbed equation corresponding to Equation (65) can be written as

$$m_I \dot{\tilde{v}}_I + \sum_{J=1}^{NP} \tilde{N}_{IJ}\, v_J + \sum_{J=1}^{NP} N_{IJ}\, \tilde{v}_J = -\tilde{f}_I^{\text{int}}. \tag{73}$$

It can be shown that Equation (73) can be expressed explicitly as

$$m_I \dot{\tilde{v}}_I + \sum_{J=1}^{NP}\left(\sum_{K=1}^{NP} m_K \tilde{\Psi}_I(x_K)\Psi_J^*(x_K)\right) v_J + \sum_{J=1}^{NP}\left(\sum_{K=1}^{NP} m_K \Psi_I(x_K)\Psi_J^*(x_K)\right)\tilde{v}_J$$
$$+ \sum_{K=1}^{NP} \tilde{\bar{B}}_I(x_K)\sigma(x_K)a_K + \sum_{K=1}^{NP} \bar{B}_I(x_K)\tilde{\sigma}(x_K)a_K + \sum_{K=1}^{NP} \bar{B}_I(x_K)\sigma_K\, \tilde{a}_K = 0. \tag{74}$$

The perturbed quantities such as $\tilde{\Psi}_I(x_K)$, $\tilde{\sigma}(x_K)$, and $\tilde{\bar{B}}_I(x_K)$ can be obtained according to their definitions. For moderate normalized support size $1 < R < 2$, by approximating $v_{I+1} = v_I + Q\Delta x$, where

$$Q = \left.\frac{\partial v}{\partial x}\right|_{x=x_I},$$

and $\tilde{v} = \dot{\tilde{u}}_I$, Equation (74) can be rewritten as

$$\ddot{\tilde{u}}_I - \frac{2Q^2[C(h)\phi_a'(h)]^2}{R^2}(\tilde{u}_{I+1} - 2\tilde{u}_I + \tilde{u}_{I-1})$$
$$+ \frac{QC(h)\phi_a'(h)}{R}\left[\Psi_I(0)(-\dot{\tilde{u}}_{I+1} + \dot{\tilde{u}}_{I-1}) + \Psi_I(h)(-\dot{\tilde{u}}_{I+2} + \dot{\tilde{u}}_{I-2})\right]$$
$$+ \frac{(C^\sigma + \sigma)}{\rho h^2}\left[C\left(\frac{h}{2}\right)\phi_a\left(\frac{h}{2}\right)\right]^2(-\tilde{u}_{I+2} + 2\tilde{u}_I - \tilde{u}_{I-2}) = 0. \tag{75}$$

Substituting Equation (62) into Equation (75) leads to

$$\omega^2 - 4Q^2\frac{[C(h)\phi_a'(h)]^2}{R^2}(1-\cos kh)$$
$$- 2Q\omega\frac{C(h)\phi_a'(h)}{R}[\Psi_I(0)\sin kh + \Psi_I(h)\sin 2kh]$$
$$- \frac{2(C^\sigma+\sigma)}{\rho h^2}\left[C\left(\frac{h}{2}\right)\phi_a\left(\frac{h}{2}\right)\right]^2(1-\cos 2kh) = 0. \tag{76}$$

Rewrite Equation (76) as

$$\omega^2 + B\omega + C = 0, \tag{77}$$

where

$$B = -2Q\frac{C(h)\phi_a'(h)}{R}[\Psi_I(0)\sin kh + \Psi_I(h)\sin 2kh]$$
$$C = -4Q^2\frac{[C(h)\phi_a'(h)]^2}{R^2}(1-\cos kh)$$
$$- \frac{2(C^\sigma+\sigma)}{\rho h^2}\left[C\left(\frac{h}{2}\right)\phi_a\left(\frac{h}{2}\right)\right]^2(1-\cos 2kh). \tag{78}$$

Define a frequency characteristic parameter $D(\omega)$ as

$$D(\omega) = B^2 - 4C. \tag{79}$$

It is observed that if $D(\omega) \geq 0$, real solution for ω is obtained and the discrete system is stable. Note that $D(\omega) \geq 0$ is satisfied as long as $C^\sigma + \sigma \geq 0$, where $C^\sigma + \sigma$ represents the tangent modulus including geometric nonlinearity effect. Therefore, under semi-Lagrangian discretization with SCNI, the sufficient condition for stability is when the tangent modulus is positive ($C^\sigma + \sigma \geq 0$). This stability condition for the semi-Lagrangian discrete system integrated by SCNI is consistent with the stability condition of a continuum.

Note that the sign of the velocity gradient Q does not affect the stability in semi-Lagrangian discretization with SCNI, hence only a non-negative velocity gradient is considered in the following study of the behavior of $D(\omega)$. Consider a discretization with uniform particle distribution, normalized support size $R = 1.5$, small velocity gradient $0 \leq Q \leq 2$, and C^σ is assumed positive.

Figure 5 demonstrates frequency characteristic parameter $D(\omega) = B^2 - 4C$ for the case where the continuum system is stable ($C^\sigma + \sigma > 0$). It can be observed from Figure 5 that in the cases when ($C^\sigma + \sigma > 0$) the frequency is real ($D(\omega) \geq 0$) for all wavelengths, representing a stable discrete system compatible with the continuum system. Figure 6 displays frequency characteristic parameter $D(\omega) = B^2 - 4C$ for the case where continuum system exhibits instability ($C^\sigma + \sigma \leq 0$). It is shown in Figure 6 that $D(\omega) < 0$ in certain range of wavelengths leading to imaginary angular frequency, and hence the discrete system is unstable. This instability in the discrete system is consistent with the continuum instability [2].

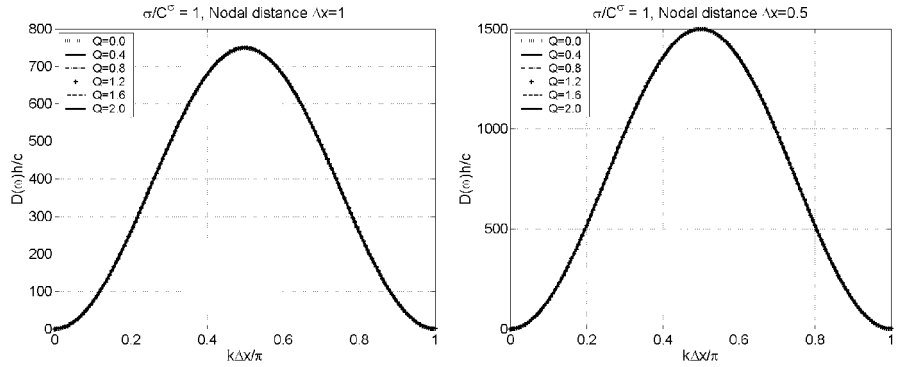

Fig. 5. Frequency characteristic parameter for semi-Lagrangian with SCNI and $C^{\sigma} + \sigma > 0$.

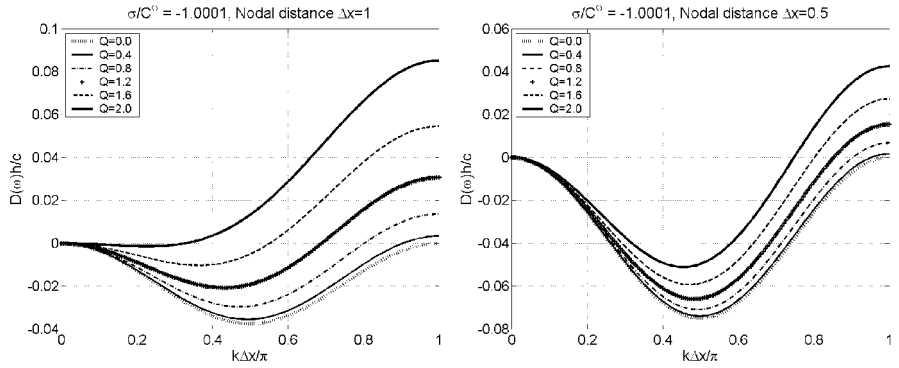

Fig. 6. Frequency characteristic parameter for semi-Lagrangian with SCNI and $C^{\sigma} + \sigma < 0$.

4.2.2 Semi-Lagrangian Weak Form Integrated by Direct Nodal Integration (DNI)

When direct nodal integration is used for domain integration, the nodal value of gradient is calculated as:

$$\bar{B}_I(x_K) = \Psi_{I,x}(x_K). \tag{80}$$

Correspondingly, Equation (74) reduces to

$$\begin{aligned}
&\ddot{\tilde{u}}_I - \frac{2Q^2[C(h)\phi_a'(h)]^2}{R^2}(\tilde{u}_{I+1} - 2\tilde{u}_I + \tilde{u}_{I-1}) \\
&\quad + \frac{QC(h)\phi_a'(h)}{R}[\Psi_I(0)(-\dot{\tilde{u}}_{I+1} + \dot{\tilde{u}}_{I-1}) + \Psi_I(h)(-\dot{\tilde{u}}_{I+2} + \dot{\tilde{u}}_{I_2})] \\
&\quad + \frac{\sigma}{\rho}\Psi_{I,xx}(h)(\tilde{u}_{I+1} - 2\tilde{u}_I + \tilde{u}_{I-1})
\end{aligned}$$

$$-\frac{(C^{\sigma}+\sigma)}{\rho}[\Psi_{I,x}(h)]^2(\tilde{u}_{I+2}-2\tilde{u}_I+\tilde{u}_{I-2})=0 \tag{81}$$

Substitution of Equation (62) into Equation (81) yields

$$\begin{aligned}\omega^2 &- 4Q^2\frac{[C(h)\phi_a'(h)]^2}{R^2}(1-\cos kh)\\ &- 2Q\omega\frac{C(h)\phi_a'(h)}{R}[\Psi_I(0)\sin kh+\Psi_I(h)\sin 2kh]\\ &+ 2\frac{\sigma}{\rho}\Psi_{I,xx}(h)(1-\cos kh)-4\frac{C^{\sigma}+\sigma}{\rho}[\Psi_{I,x}(h)]^2\sin^2(kh)=0.\end{aligned} \tag{82}$$

Equation (82) can be written as

$$\omega^2+B\omega+A=0, \tag{83}$$

where B is given in Equation (78), and

$$\begin{aligned}A=&\left\{-4Q^2\frac{[C(h)\phi_a'(h)]^2}{R^2}+2\frac{\sigma}{\rho}\,\Psi_{I,xx}(h)\right\}(1-\cos kh)\\ &-4\frac{C^{\sigma}+\sigma}{\rho}[\Psi_{I,x}(h)]^2\sin^2(kh).\end{aligned} \tag{84}$$

Define the frequency characteristic parameter $D(\omega)$ as

$$D(\omega)=B^2-4A. \tag{85}$$

Note that the sign of $\sigma\Psi_{I,xx}(h)$, and hence the sign of stress σ, plays an important role in the stability of discrete system integrated by DNI.

In the stability analysis shown below, discretization with constant nodal distance $\Delta x=0.05$ is employed. Figures 7 and 8 demonstrate frequency characteristic parameter $D(\omega)=B^2-4A$ for different values of Q and σ/C^{σ}. The results in Figure 7 show that when a stable continuum is under tension ($C^{\sigma}+\sigma>0$), imaginary frequency occurs ($D(\omega)<0$) at certain wavelengths, leading to an unstable discrete system constructed using DNI. This is referred to as the tensile instability observed in SPH [20]. On a separate test as shown in Figure 8, the discrete system constructed using DNI becomes stable when continuum instability occurs ($C^{\sigma}+\sigma\leq 0$), and it is unphysical.

4.3 Effect of Convective Term on Stability

To examine how the convective term in the semi-Lagrangian discretization affects the stability of the discrete equation, consider removing the convective term (second

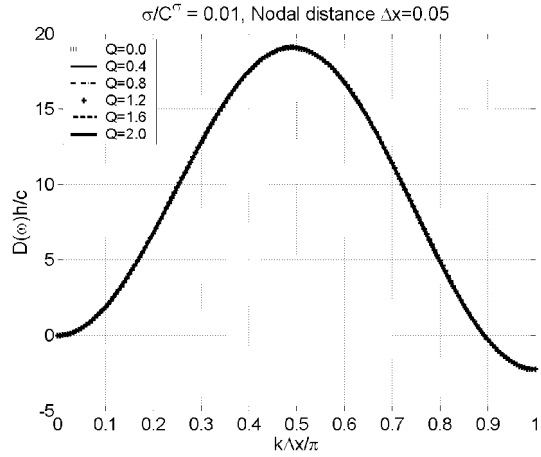

Fig. 7. Frequency characteristic parameter for semi-Lagrangian with DNI for $C^{\sigma} + \sigma > 0$ and $\sigma > 0$.

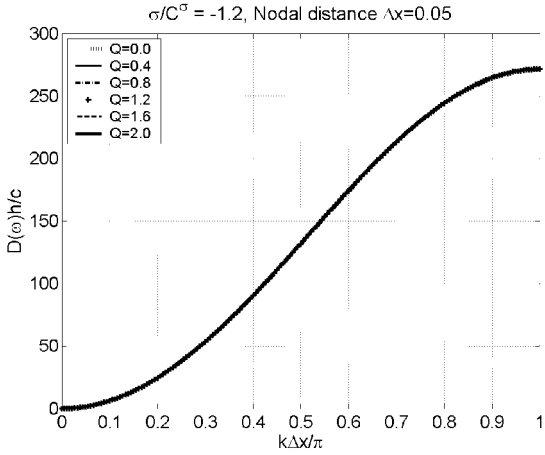

Fig. 8. Frequency characteristic parameter for semi-Lagrangian with DNI for $\sigma + C^{\sigma} < 0$.

term in Equation (65)) to yield the following dispersion equations constructed by SCNI and DNI:

(1) SCNI

$$\omega^2 - \frac{2(C^{\sigma} + \sigma)}{\rho h^2}\left[C\left(\frac{h}{2}\right)\phi_a\left(\frac{h}{2}\right)\right]^2 (1 - \cos 2kh) = 0 \tag{86}$$

(2) DNI (equivalent to SPH)

$$\omega^2 = 2\frac{C^\sigma + \sigma}{\rho}[\Psi_{I,x}(h)]^2\,(1-\cos 2kh) - 2\frac{\sigma}{\rho}\,\Psi_{I,xx}(h)(1-\cos kh). \qquad (87)$$

By comparing Equations (76) and (86) for the semi-Lagrangian discretization integrated by SCNI, it is seen that inclusion of the convective term in the semi-Lagrangian discretization does not have negative influence on the stability property of discrete system. In fact, the stability is slightly improved when convective term is included in the semi-Lagrangian discrete equation. Similar situation is observed by comparing Equations (82) and (87) for the DNI case.

Equation (86) confirms that there is no tensile instability if SCNI is employed in the semi-Lagrangian discretization. On the other hand, it is seen from Equation (87) that if DNI is employed, tensile instability will occur. This tensile instability condition in Equation (87) when $\sigma\Psi_{I,xx}(h) > 0$ reflects tensile instability in SPH as has been identified by Swegle et al. [20]. Based on the stability analysis of semi-Lagrangian discretization in Sections 4.2.1 and 4.2.2 and in this section, it is shown that SCNI always yields a stable semi-Lagrangian discrete system regardless of the inclusion of convective term if the continuum is stable, whereas instability is observed when DNI is employed.

Note that the semi-Lagrangian discrete equation constructed with DNI and with convective term removed yields an SPH type formulation. By comparing Equation (76) (semi-Lagrangian discretization integrated by SCNI and with convective term included) and Equation (87) (semi-Lagrangian discretization integrated by DNI and without convective term included, representing SPH), it is suggested the stability of SPH can be improved by introducing strain smoothing of SCNI in the nodal strain calculation and by including the convective term in the SPH equation of motion.

5 Conclusions

Lagrangian formulation breaks down when the one-to-one mapping of material point position between undeformed domain and deformed domain cannot be defined. This situation happens in the processes of new free surface formation in damage evolution or free surface closure that commonly exists in materials processing, earth moving, and penetration processes. To circumvent this difficulty, a semi-Lagrangian discretization is proposed. In the Lagrangian discretization the distance measure in the kernel function is defined in the initial undeformed domain, whereas in the semi-Lagrangian discretization the distance measure in the kernel function is defined in the current deformed domain. It has been shown that the semi-Lagrangian discretization yields a convective term resulting from the non-conservative coverage of material points under the kernel support.

Von Neumann stability analyses have been performed for Reproducing Kernel (RK) Lagrangian and semi-Lagrangian discretizations with weak forms integrated

using stabilized conforming nodal integration (SCNI). In Lagrangian discretization with SCNI, the stability of the discrete system is always consistent with the stability of the continuum. In the semi-Lagrangian discrete equation, an additional convective term exists due to the change of material particles covered under the semi-Lagrangian kernel function during different states of material deformation. By comparison of stability conditions of Lagrangian and semi-Lagrangian discretizations integrated by SCNI, it has been shown that the inclusion of the convective term in the semi-Lagrangian discretization offers a slightly better stability compared to the semi-Lagrangian discretization without convective term. The stability analysis also showed similar stability conditions between Lagrangian and semi-Lagrangian discretizations if convective term is included in the semi-Lagrangian discretization.

The stability of semi-Lagrangian discretization with domain integration by a direct nodal integration (DNI) has also been analyzed. The analysis results demonstrated that semi-Lagrangian discretization constructed by DNI yields instability under tension, which is referred to as the tensile instability in SPH. Note that semi-Lagrangian discretization integrated by DNI and with removal of convective term resembles SPH. The stability analysis performed in this work suggests that the stability of SPH can be improved with the addition of convective term in the equation of motion and by introducing strain smoothing employed in SCNI in the nodal strain evaluation of SPH.

Acknowledgement

The support of this work by Lawrence Livermore National Laboratory to University of California, Los Angeles, is greatly acknowledged.

References

1. Belytschko T. and Xiao S.P. Stability analysis of particle methods with corrected derivatives. *Computers and Mathematics with Applications*, 43:329–350, 2002.
2. Belytschko T., Guo Y., Liu W.K. and Xiao S.P. A unified stability analysis of meshless particle methods. *International Journal for Numerical Methods in Engineering*, 48:1359–1400, 2000.
3. Bonet J. and Kulasegaram S. Remarks on tension instability of Eulerian and Lagrangian corrected smooth particle hydrodynamics (CSPH) methods. *International Journal for Numerical Methods in Engineering*, 52:1203–1220, 2001.
4. Chen J.S., Pan C. and Wu C.T. Large deformation analysis of rubber based on a reproducing kernel particle method. *Computational Mechanics*, 19:211–217, 1997.
5. Chen J.S., Pan C., Roque C. and Wang H.P. A Lagrangian reproducing kernel particle method for metal forming analysis. *Computational Mechanics*, 22:289–307, 1998.
6. Chen J.S., Pan C., Wu C.T. and Liu W.K. Reproducing kernel particle methods for large deformation analysis of non-linear structures. *Computer Methods in Applied Mechanics and Engineering*, 139:195–227, 1996.

7. Chen J.S., Roque C.M.O.L., Pan C. and Button S.T. Analysis of metal forming process based on meshless method. *Journal of Materials Processing Technology*, 80/81:642–646, 1998.
8. Chen J.S., Wu C.T. and Belytschko T. Regularization of material instability by meshfree approximations with intrinsic length scales. *International Journal for Numerical Methods in Engineering*, 47:1301–1322, 2000.
9. Chen J.S., Wu C.T., Yoon S. and You Y. A stabilized conforming nodal integration for Galerkin mesh-free methods. *International Journal for Numerical Methods in Engineering*, 50:435–446, 2001.
10. Chen J.S., Yoon S. and Wu C.T. Non-linear version of stabilized conforming nodal integration for Galerkin mesh-free methods. *International Journal for Numerical Methods in Engineering*, 53:2587–2615, 2002.
11. Chen J.S., Yoon S., Wang H.P. and Liu W.K. An improved reproducing kernel particle method for nearly incompressible hyperelastic solids. *Computer Methods in Applied Mechanics and Engineering*, 181:117–145, 2000.
12. Gingold R.A. and Monaghan J.J. Smoothed particle hydrodynamics: Theory and application to non-spherical stars. *Monthly Notices of the Royal Astronomical Society*, 181:375–389, 1977.
13. Lancaster P. and Salkauskas K. Surfaces generated by moving least-squares methods. *Mathematics of Computation*, 37:141–158, 1981.
14. Liu W.K., Jun S. and Zhang Y.F. Reproducing kernel particle methods. *International Journal for Numerical Methods in Fluids*, 20:1081–1106, 1995.
15. Lucy L.B. A numerical approach to the testing of the fission hypothesis. *The Astronomical Journal*, 82:1013–1024, 1977.
16. Libersky L.D. and Petschek A.G. Smooth particle hydrodynamics with strength of materials. In: *Advances in the Free Lagrange Method*, Lecture Notes in Physics, Vol. 395, Springer-Verlag, 1990.
17. Monaghan J.J. SPH without a tensile instability. *Journal of Computational Physics*, 159:290–311, 2000.
18. Rabczuk T., Belytschko T. and Xiao S.P. Stable particle methods based on Lagrangian kernels. *Computer Methods in Applied Mechanics and Engineering*, 193:1035–1063, 2004.
19. Randles P.W. and Libersky L.D. Smoothed particle hydrodynamics: Some recent improvements and applications. *Computer Methods in Applied Mechanics and Engineering*, 139:375–408, 1996.
20. Swegle J.W., Hicks D.L. and Attaway S.A. Smoothed particle hydrodynamics stability analysis. *Journal of Computational Physics*, 116:123–134, 1995.
21. Dyka C.T. and Ingel R.P. An approach for tension instability in smoothed particle hydrodynamics. *Computers & Structures*, 57:573–580, 1995.
22. Guenther C., Hicks D.L. and Swegle J.W. Conservative smoothing versus artificial viscosity. Sandia Report SAND94-1853, Sandia National Lab., 1994.
23. Swegle J.W., Attaway S.W., Heinstein M.W., Mello F.J. and Hicks D.L. An analysis of smoothed particle hydrodynamics. Sandia Report SAND94-2513, Sandia National Lab., 1994.